Block-based mismatched filters for self-interference mitigation in PMCW radars

Çağan Önen
NXP Semiconductors
Eindhoven, The Netherlands
cagan.onen_1@nxp.com

Hanqing Wu
NXP Semiconductors
Eindhoven, The Netherlands
hanqing.wu@nxp.com

Ashish Pandharipande
NXP Semiconductors
Eindhoven, The Netherlands
ashish.pandharipande@nxp.com

***Abstract*—Phase modulated continuous wave (PMCW) radars are an attractive solution in automotive driving applications due to waveform flexibility in digital designs. Self-interference in PMCW radars however limits the dynamic range due to resulting sidelobes, and conventional matched filters used for range processing at the radar receiver has degraded detection performance. To tackle this problem, we propose a block-based mismatched filter (MMF) design to partition the radar range into multiple zones and suppress the sidelobes in these regions in parallel. By considering diverse automotive application scenarios, we show that the presented MMF design achieves better detection performance than the conventional matched filter approach in the presence of self-interference.**

***Index Terms*—PMCW radar, Mismatched filters, Self-interference mitigation.**

I. Introduction

Radar is a critical sensor technology for robust scene understanding in an advanced driver assistance system (ADAS) [1]–[3]. As the functionalities offered in ADAS evolve, there is a need to support flexible waveforms to support diverse application requirements as well as deal with automotive radar interference. PMCW radars have recently gained attention as a flexible digital radar solution with higher immunity to interference across automotive radars [4]–[6].

In a PMCW radar, range estimation is conventionally carried out using a matched filter (MF), wherein the received signal is correlated with the transmitted codeword to extract the target delays [4]. Ideally, an autocorrelation function should exhibit a sharp peak with negligible sidelobes. However, binary sequences impose phase constraints that prevent perfect sidelobe suppression, resulting in residual correlation energy distributed along the range profile. As a result, strong targets create high sidelobes masking the weaker ones. This problem is dominant due to direct leakage from the transmitter to the receiver antennas leading to self-interference (SI), and appears in the zero Doppler bin. Since the leakage maintains a direct correlation with the transmitted codeword experiencing negligible path loss, a strong response with sidelobes reaching several orders of magnitude stronger than typical target echoes is created [7], [8]. In other Doppler bins, sidelobes levels are elevated due to the Doppler shift induced by the relative motion of the targets, which degrades the orthogonality of the signal and alters the theoretically provided sidelobe levels [9].

In comparison to MFs that maximize single target SNR, a mismatched filter (MMF) is a signal processing filter designed to optimize performance metrics, such as integrated sidelobe ratio (ISLR) and peak to sidelobe ratio (PSLR) [10]–[13]. A MMF has been shown to be effective in suppressing the range sidelobes within a limited low correlation zone (LCZ) with a small decrease in SNR. However, the SNR loss increases with the size of the LCZ, making this approach not suitable for spanning the entire range spectrum.

We propose a block-based MMF design with multiple, distinct LCZs spanning the entire range bins. Each MMF is designed to suppress sidelobes in a LCZ, resulting in sidelobe suppression due to SI throughout the range spectrum, at the expense of a small decrease in SNR. In the design of individual MMFs, while we adopt the ISLR-minimizing approach proposed in [10] due to its closed-form solution, our block-based MMF design approach is more generally applicable to a broad class of MMFs.

We evaluate our block-based MMF method based on detection performance and sidelobe suppression capability and compare it with the conventional MF-based range processing. In different automotive driving application simulation scenarios, we show that the proposed design offers better suppression of SI sidelobes leading to better detection of weak targets, thereby achieving higher probability of detection.

II. PMCW Radar System Model

A block diagram of a binary PMCW radar system is illustrated in Fig. 1. A continuous RF carrier modulated by binary sequences $\boldsymbol{x} = [x(0), x(1), \ldots, x(S-1)] \in \mathbb{R}^S$ is transmitted, where $x(n) \in \{1, -1\}$ representing 0° or 180° phase shifts, respectively. Pseudo-random binary sequences with good correlation properties modulate the phase of a

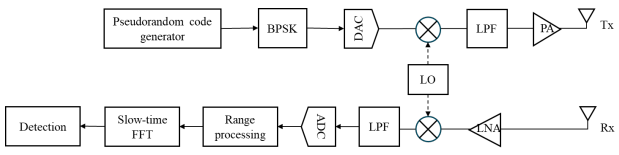

Fig. 1: PMCW radar block diagram

carrier f_c. Repeating the sequence N times in slow time within one frame forms the transmit signal:

$$s_T(t) = \sum_{n=0}^{N-1} \sum_{s=0}^{S-1} x(s) \cos(2\pi f_c t) \text{rect}\left(\frac{t - nT - sT_c}{T_c}\right) \quad (1)$$

where T_c is the chip duration, inversely proportional to the bandwidth of the transmitted signal, $T_c = \frac{1}{B}$, $T = ST_c$ is the code repetition interval and $\text{rect}(.)$ is the rectangular function that has a value of 1 between 0 and 1, and 0 otherwise.

Range processing in PMCW radars is perfomed by correlating the received ADC samples $\boldsymbol{r} = [r(0), r(1), \ldots, r(S-1)] \in \mathbb{C}^S$ with a reference filter to estimate signal delays from target reflections. The filter is denoted as $\boldsymbol{y} = [y(0), y(1), \ldots, y(S-1)] \in \mathbb{R}^S$, and the correlation output is given by

$$c_{r,y}(\tau) = \sum_{n=0}^{S-1} r(n) y((n-\tau) \bmod S). \quad (2)$$

where $\tau \in [0 : S-1]$ represents discrete delay shifts. Peaks in the correlation result indicate time-of-flight reflections, enabling range estimation. Conventionally, matched filtering is employed, where the receiver filter $\boldsymbol{y}$ is identical to the transmitted sequence $\boldsymbol{x}$, producing peak values proportional to S. Following range estimation, target velocities are resolved via an N-point FFT in slow time. The range-Doppler output is then processed by a constant false alarm rate (CFAR) detector for target detection.

III. Block-based MMF Processing and Detection Method

The block-based mismatched filter (MMF) design involves partitioning the range spectrum into B equally sized blocks and applying a set of B mismatched filters, $\{\boldsymbol{y}_b\}_{b=1}^{B} = [y_b(0), y_b(1), \ldots, y_b(S-1)] \in \mathbb{R}^S$, to suppress sidelobes within each respective block. Each MMF is designed to perform local sidelobe suppression inside an LCZ. The LCZ of the b^{th} block, for $b = 1, 2, \cdots, B$, containing L range bins, can be defined as

$$\mathcal{L}_b = \{(\frac{(b-2)L}{2} + i) \bmod S \mid i = 0, 1, \cdots, L-1\}. \quad (3)$$

To ensure seamless coverage of the range spectrum, the B LCZs collectively span all range bins while maintaining localized sidelobe suppression within each LCZ. This overlapping strategy ultimately improves the overall reliability of the block-based MMF processing framework, as illustrated in Figure 2. The received ADC samples $\boldsymbol{r}$ undergo correlation with B mismatched filters $\boldsymbol{y}_b$, each corresponding to a distinct LCZ $\mathcal{L}_b$. The outputs are stored in a buffer, accumulating N slow-time samples before undergoing Doppler processing via a slow-time FFT. Detection is then applied to each block's range-Doppler map (RDM), and the detected set $\mathcal{D}_b$ from all blocks are fused to obtain the final detection set $\mathcal{D}_{final}$.

A. Block-based MMF design

In this work, we use an ISLR-minimizing approach to reduce the integrated sidelobe energy inside each LCZ, thereby enhancing the dynamic range and improving weak-signal detection. This method is particularly advantageous as it ensures uniform sidelobe suppression, preventing localized interference variations. To quantify this, the integrated sidelobe energy within the b^{th} block is given as $\boldsymbol{y}_b^H \boldsymbol{P}_b \boldsymbol{y}_b$, where

$$\boldsymbol{P}_b = \sum_{k \in \mathcal{L}_b} \boldsymbol{x}_k \boldsymbol{x}_k^H \in \mathbb{R}^{S \times S}, \quad (4)$$

and $\boldsymbol{x}_k$ be the k-sample circularly shifted version of $\boldsymbol{x}$.

Now the MMF design optimization problem for block b can be written as

$$\begin{aligned} \min_{\boldsymbol{y}_b} \quad & \boldsymbol{y}_b^H \boldsymbol{P}_b \boldsymbol{y}_b \\ \text{s.t.} \quad & \boldsymbol{y}_b^H \boldsymbol{y}_b = S, \\ & |c_{x,y_b}(0)| \geq \alpha S, \end{aligned} \quad (5)$$

where the first constraint eliminates the trivial solution and the second constraint limits the SNR loss to $-20\log_{10}\alpha$ dB where $0 < \alpha < 1$.

To solve (5), we first disregard the second constraint. A closed-form solution to this problem is proposed in [10]. The solution is based on choosing a $\boldsymbol{y}_b$ that lies in the null space of $\boldsymbol{P}_b$. Since $\boldsymbol{P}_b$ is positive semidefinite, its null space represents the components that do not contribute to the integrated sidelobe energy within the LCZ. To preserve most of the signal components and to ensure minimal SNR loss, $\boldsymbol{y}_b$ is constructed as the projection of $\boldsymbol{x}$ to null($\boldsymbol{P}_b$) as

$$\boldsymbol{y}_b = \frac{1}{\sigma_b} \sum_{m=1}^{M} \boldsymbol{u}_{b,m}^H \boldsymbol{x} \boldsymbol{u}_{b,m}, \quad (6)$$

$$\sigma_b = \sqrt{\frac{\sum_{m=1}^{M} |\boldsymbol{u}_{b,m}^H \boldsymbol{x}|^2}{S}}, \quad (7)$$

where $-20\log_{10}\sigma_b$ is the resultant SNR loss and $\{\boldsymbol{u}_{b,m}\}_{m=1}^{M} \in \mathbb{R}^S$ are the eigenvectors corresponding to the zero eigenvalues of $\boldsymbol{P}_b$.

Now, if the obtained solution does not satisfy the second constraint in (5), we reduce L till the obtained σ_b satisfies this constraint. A lower value of L reduces Rank($\boldsymbol{P}_b$) and enlarges the null space of $\boldsymbol{P}_b$. Note that each row of $\boldsymbol{P}_b$ is a linear combination of $|\mathcal{L}_b| = L$ different circular shifted versions of a binary sequence according to (4) which makes Rank($\boldsymbol{P}_b$) $\leq L$ (in our case, we consider Gold sequences whose circular shifts are empirically observed to be linearly independent). A lower rank expands the null space of $\boldsymbol{P}_b$, providing more freedom for $\boldsymbol{x}$ to be projected, and thus leading to a higher value of σ_b from the new MMF design solution.

B. Detection and fusion

After Doppler processing with an N-point FFT, each block generates a corresponding RDM_b, which is then processed by a peak detector followed by CFAR detection. The peak

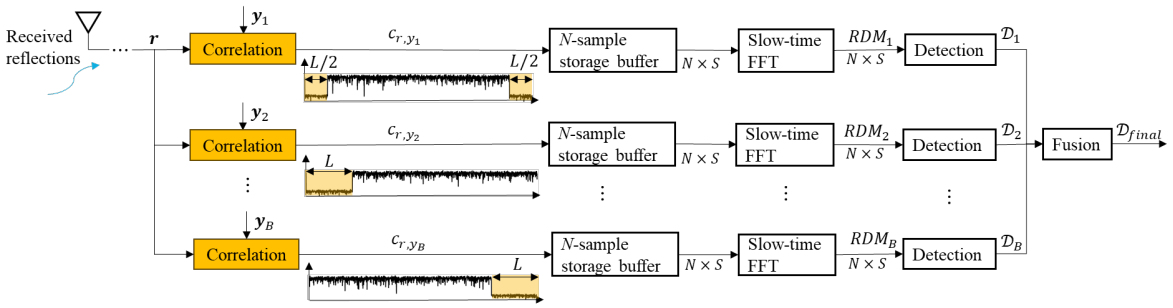

Fig. 2: Block-based MMF with overlapping LCZs, Doppler processing and detection.

detector scans RDM_b and identifies bins whose values exceed those of their immediate neighbors along both axes. These identified peaks are then passed to the CFAR detector, which dynamically estimates the noise floor using surrounding reference cells and applies an adaptive threshold for detection. This process yields a detected target set $\mathcal{D}_b$ for each block. The final detection set $\mathcal{D}_{\text{final}}$ is obtained by taking the union of all $\mathcal{D}_b$ across blocks as $\mathcal{D}_{\text{final}} = \bigcup_{b=1}^{B} \mathcal{D}_b$.

Due to the fusion of detections from multiple blocks, false alarms become a critical issue, particularly at the edges of LCZs. To mitigate this, we adopt the greatest-of CFAR (GO-CFAR) approach, which sets the detection threshold based on the higher noise level from both sides of the target bin [14].

A key consequence of this fusion-based approach is the increased computational load. Unlike conventional MF processing, which requires a single Doppler processing and detection step, the block-based MMF system requires B Doppler processing steps and B detections to each block's RDM. This results in an overall increase in computational complexity by a factor of B.

IV. Simulation Results

We now evaluate the sidelobe suppression capability and the detection performance of the proposed approach in comparison with conventional MF-based processing. We consider a SISO long-range PMCW radar system at a carrier frequency of 77 GHz with a bandwidth of 1 GHz using a Gold sequence of length 2047 and $N = 2048$ in the simulations. We simulate SI-enabled scenarios with a transmitter-to-receiver leakage of 30 dB attenuation relative to the 12 dBm transmitted power.

A. Simulation setup

We provide a qualitative comparison based on the resultant RDMs and detections. Besides, we adopt Mean Sidelobe Level (MSL) for quantitative evaluation which is calculated at the Doppler bin k as:

$$\text{MSL}(k) = 20\log_{10}\left(\frac{1}{|\Omega|}\sum_{n\in\Omega\setminus\mathcal{T}}|RDM(n,k)|\right). \quad (8)$$

Here, Ω denotes the set of range bins over which the metric is computed, while $\mathcal{T}$ represents the target indices that are excluded from the calculation. The performance of the MMF in the LCZs is reflected by choosing $\Omega = \mathcal{L}_b$.

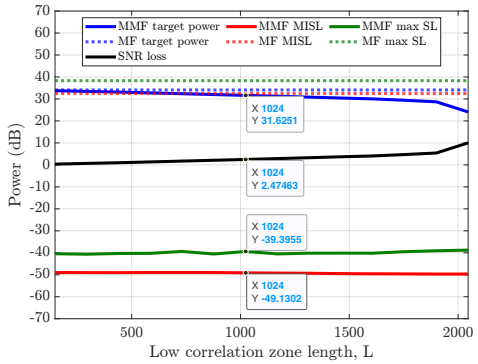

Fig. 3: MSL and target power values for various values of L.

The MMF parameter, L, determines the sidelobe suppression capability and the number of LCZ blocks required in the system. The value of integer L can be chosen between 0 and S based on the maximum tolerable SNR loss. The experiment is carried out with a single stationary 25 dBsm target at 5 m. Fig. 3 shows the target power and sidelobe levels inside the LCZ for various values of L, in comparison with the MF. Sidelobe levels can be seen almost constant inside the LCZ, and SNR loss increases with L. Thus, if enough computational resources are available, SNR loss can be kept low by choosing a low L, and thus larger B. Here, we fix the maximum allowable SNR loss at 2.5 dB, and choose $L = 1024$ and $B = 4$ with 50% overlap. By overlapping adjacent LCZs, we enhance transitions between MMFs and mitigate target loss at LCZ edges.

B. Discussion of results

1) Near-Far (NF) Scenario: In this scenario, we evaluate the radar system's capability to detect distant targets in the presence of nearby target. In this setup, a car with radar cross section (RCS) of 15 dBsm is positioned at 10 meters, while a truck with RCS of 25 dBsm is located at 200 meters. Both targets have a relative velocity of 0 m/s.

The range cut comparison in Fig. 4 shows that the MF approach yields an MSL of 19.8 dB, preventing target detection. In contrast, the MMF approach achieves an MSL of -51.0 dB in the corresponding LCZ, effectively suppressing sidelobe levels. With a GOCA-CFAR detector designed at $P_{fa} = 5\times10^{-9}$, this suppression enables successful detection

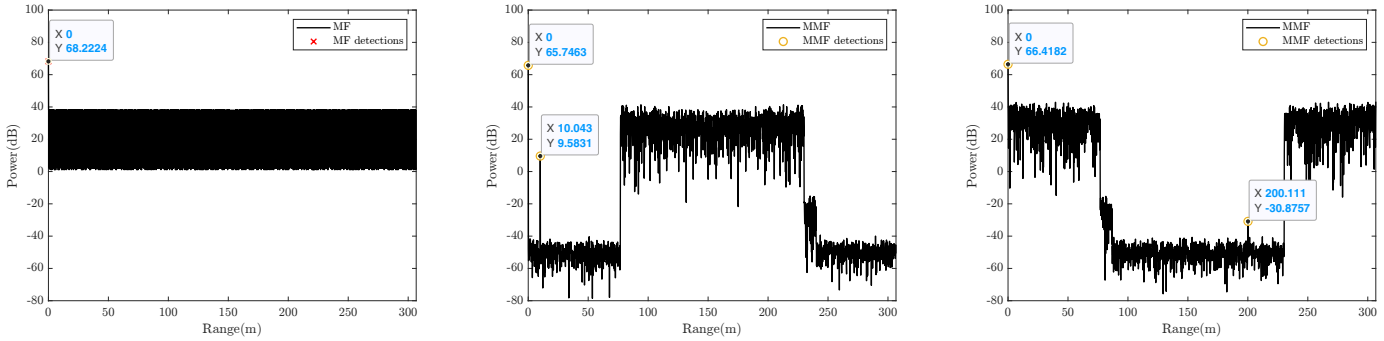

(a) MF range cut

(b) MMF range cut ($b = 1$)

(c) MMF range cut ($b = 3$)

Fig. 4: NF range cuts: MF vs MMF.

of both targets in block one and block three, respectively. These findings demonstrate the improved ability of the block-based MMF technique in mitigating SI sidelobes and enhancing target detection in the NF scenario.

2) High contrast resolution (HCR) scenario: This scenario involves four targets with distinct RCS: two trucks (25 dBsm) at 25 meters and two adjacent weak targets (-10 dBsm) at 24.5 meters. Truck 1 and weak target 1 are stationary, while Truck 2 and weak target 2 move at 30 m/s.

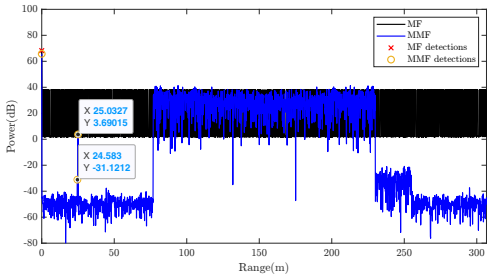

(a) Range cut comparison at 0 m/s.

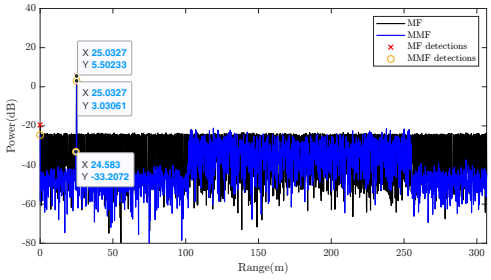

(b) Range cut comparison at 30 m/s.

Fig. 5: HCR range cuts comparison: MF vs MMF.

Fig. 5a presents the range cut comparison at 0 m/s. When applying MF, no targets are detected due to strong sidelobes induced by SI, resulting in an MSL of 19.8 dB, which obscures targets. In contrast, the MMF approach significantly reduces the MSL to -50.2 dB within the LCZ ($b = 1$), achieving an approximate improvement of 70 dB. Consequently, the MMF approach successfully detects both targets at 0 m/s. At 30 m/s (Fig. 5b), the MF approach successfully detects the truck but fails to detect the weak target due to elevated sidelobe levels caused by the strong truck signal. The MF method exhibits an MSL of -36.6 dB, whereas MMF decreases the MSL to -49.5 dB in the LCZ, providing a 13 dB enhancement. Furthermore, a comparison of target power between MF and MMF reveals a difference of within 2.5 dB, which aligns with the expected SNR loss when applying MMF. These results demonstrate that MMF effectively suppresses sidelobes caused by both SI and Doppler phase shifts while maintaining an acceptable SNR loss. As a result, the proposed MMF enhances target detection in HCR scenarios.

3) Highway scenario: This simulation uses a highway scenario to evaluate the performance of the proposed MMF in a complex environment with multiple targets. Fig. 6a illustrates the distribution of 100 targets in range and velocity, with their RCS represented using a color bar for clarity.

In the RDM shown in Fig. 6b, a sidelobe ridge can be observed around the zero Doppler bin when applying MF. By examining the RDM with 4 MMFs across different blocks, we clearly see that the sidelobe attenuation effect in these blocks. We set CFAR-designed P_{fa} as 5×10^{-9}. In the MF approach, a total of 48 targets are correctly detected. In contrast, in the MMF approach, the detected targets are the union of the targets identified in each block, resulting in an improved total of 84 detected targets. A comparison of the receiver operating characteristic (ROC) curves shown in Fig. 7 reveals that the proposed approach achieves higher P_d in comparison to the MF based approach for practical values of P_{fa}.

V. Conclusions

Sidelobe suppression using a block of ISLR-minimizing MMFs was proposed. Under the considered simulation scenarios, better detection performance of MMF over conventional MF was observed in three aspects. First, suppression of high cross-correlation sidelobes resulting from SI is achieved across the entire range bins. This enhancement enables detection of smaller objects in the zero Doppler cut. Second, our method is able to detect farther targets even in the presence of nearby large targets at the same velocity. This improvement extends the maximum detection range while also achieving a higher dynamic range. Finally, better detection performance is

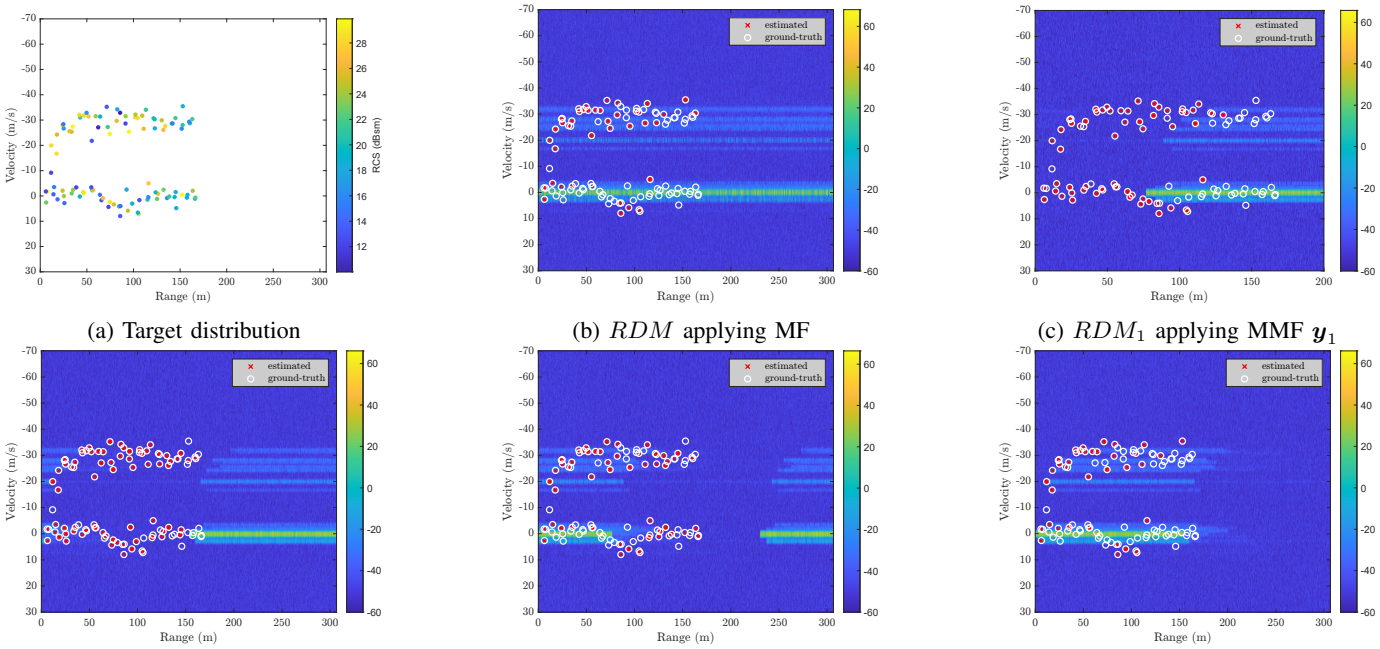

(a) Target distribution

(b) RDM applying MF

(c) RDM_1 applying MMF $\boldsymbol{y}_1$

(d) RDM_2 applying MMF $\boldsymbol{y}_2$

(e) RDM_3 applying MMF $\boldsymbol{y}_3$

(f) RDM_4 applying MMF $\boldsymbol{y}_4$

Fig. 6: Highway target distribution & RDMs: MF vs MMF.

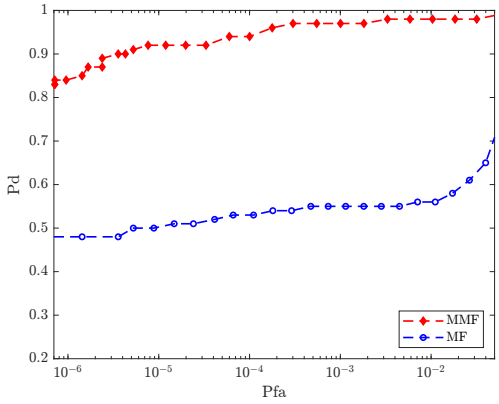

Fig. 7: ROC comparison.

observed in a highway scenario with a large number of targets with diverse velocities and high RCS values.

The use of multiple blocks of MMFs for range processing and slow-time FFTs increases the overall system complexity. An extended version of this work will present fusion approaches to reduce range-Doppler processing complexity.

References

[1] F. Engels, P. Heidenreich, M. Wintermantel, L. Stäcker, M. Al Kadi, and A. M. Zoubir, "Automotive Radar Signal Processing: Research Directions and Practical Challenges," *IEEE Journal of Selected Topics in Signal Processing*, vol. 15, no. 4, pp. 865–878, 2021.

[2] G. Hakobyan and B. Yang, "High-performance automotive radar: A review of signal processing algorithms and modulation schemes," *IEEE Signal Processing Magazine*, vol. 36, no. 5, pp. 32–44, 2019.

[3] A. Pandharipande, C.-H. Cheng, J. Dauwels, S. Z. Gurbuz, J. Ibanez-Guzman, G. Li, A. Piazzoni, P. Wang, and A. Santra, "Sensing and machine learning for automotive perception: A review," *IEEE Sensors Journal*, vol. 23, no. 11, pp. 11 097–11 115, 2023.

[4] D. Guermandi, Q. Shi, A. Dewilde, V. Derudder, U. Ahmad, A. Spagnolo, I. Ocket, A. Bourdoux, P. Wambacq, J. Craninckx, and W. Van Thillo, "A 79-GHz 2 × 2 MIMO PMCW Radar SoC in 28-nm CMOS," *IEEE Journal of Solid-State Circuits*, vol. 52, no. 10, pp. 2613–2626, 2017.

[5] Y. Chen, Y. Cheng, R. Lin, H. C. So, and J. Li, "Joint Design of Binary Probing Sequence Sets and Receive Filter Banks for MIMO PMCW Radar," *IEEE Transactions on Signal Processing*, vol. 72, pp. 1620–1633, 2024.

[6] R. Amar, M. Ahmadi, M. Alaee-Kerahroodi, M. R. Bhavani Shankar, and B. Ottersten, "USRP based Implementation of Interference Immune PMCW Radars with Low Sampling rate ADCs," in *2024 21st European Radar Conference (EuRAD)*, 2024, pp. 55–58.

[7] M. Bauduin and A. Bourdoux, "Mixed-Signal Transmitter Leakage Cancellation for PMCW MIMO Radar," in *2018 15th European Radar Conference (EuRAD)*, 2018, pp. 293–296.

[8] P. Stagnaro, A. Pandharipande, J. Overdevest, and H. Joudeh, "Mimo digital radar processing with spatial nulling for self-interference mitigation," in *2023 IEEE Sensors*, 2023, pp. 1–4.

[9] J. Overdevest, F. Jansen, F. Uysal, and A. Yarovoy, "Doppler Influence on Waveform Orthogonality in 79 GHz MIMO Phase-Coded Automotive Radar," *IEEE Transactions on Vehicular Technology*, vol. 69, no. 1, pp. 16–25, 2020.

[10] R. Lin, Z. Liu, Y. Chen, H. C. So, and J. Li, "Theoretical Insights and Practical Algorithms for Transceiver Design of PMCW Radar," *IEEE Transactions on Signal Processing*, vol. 72, pp. 3091–3103, 2024.

[11] A. Sakhnini, M. Bauduin, A. Bourdoux, and S. Pollin, "Mismatched Filters for High-Velocity Target Detection in PMCW Radars," in *2023 20th European Radar Conference (EuRAD)*, 2023, pp. 114–117.

[12] O. Rabaste and L. Savy, "Mismatched filter optimization for radar applications using quadratically constrained quadratic programs," *IEEE Transactions on Aerospace and Electronic Systems*, vol. 51, no. 4, pp. 3107–3122, 2015.

[13] T. Aittomäki and V. Koivunen, "Mismatched Filter Design and Interference Mitigation for MIMO Radars," *IEEE Transactions on Signal Processing*, vol. 65, no. 2, pp. 454–466, 2017.

[14] M. A. Richards, *Fundamentals of Radar Signal Processing*. McGraw-Hill Professional, 2005.